

Impurity bands, magnetic ordering, and metal–insulator transitions in dielectrics doped with transitional metals

A. I. Agafonov and É. A. Manykin

Kurchatov Institute Russian Research Center, 123182 Moscow, Russia

(Submitted 18 June 1995)

Zh. Éksp. Teor. Fiz. **109**, 1405–1419 (April 1996)

We have used the Anderson model to describe the modifications in the energy spectrum and phase diagram of nonmagnetic dielectrics due to doping with magnetic impurities. The ground state was derived from the Green's functions averaged over ensembles of impurities randomly distributed through the host lattice in the Hartree–Fock approximation with the Fermi energy determined self-consistently. Narrow, continuous impurity bands are generated with a high density of states, which are spin-degenerate only when the impurity atoms form a paramagnetic. An important point is that high-concentration peaks due to localized states belong to these bands. The positions of the impurity bands, and their density of states and population are strong functions of the impurity concentration. When there is one electron per impurity, a magnetic insulating state is formed at low concentrations, although there is another solution, which describes a paramagnetic metal. As the impurity concentration increases, the material sequentially transforms to two conducting phases, one of which is magnetic and the other paramagnetic, with a gradual transition between them. © 1996 American Institute of Physics. [S1063-7761(96)02504-8]

1. INTRODUCTION

Presently quantum phase transitions are defined as transformations taking place at low temperatures when fluctuations which control the critical behavior of the system are not of thermal, but of quantum origin.¹ These phase transitions are classified in two categories.^{1,2} In the first category, changes in the lattice due to a structural phase transition split energy bands that may lead to a metal–insulator transition in a solid. The second category includes purely electronic transitions. These transitions are usually described either by a model with a fixed crystal lattice or by a model with disorder. The latter case is known as the Anderson transition.³

The Hubbard and Anderson lattice models are most often used to study strongly correlated electron systems.^{4–7} In these models the structure of the electron energy bands is controlled by the lattice of the host material, and impurities only change their energies and populations, and hence the Fermi energy. As the occupation of the bands is varied, an insulator–metal transition takes place. This process is classified as the Mott–Hubbard transition.

Naturally, the role of impurities is not limited to changing the total number of carriers in the system. The perturbations due to impurities may notably change the electronic spectrum of the crystal. The combined effect of disorder and strong correlations among electrons on the phase diagram was studied by several researchers using lattice models.^{8–11} Some parameters of the model were treated as random independent variables.

Formation of impurity bands in the energy gap of a dielectric doped with transitional metal atoms from extended and localized states was also studied.¹² The model Hamiltonian took into account potential scattering of band electrons from impurities randomly distributed through the lattice and hybridization between band states of the dielectric

spectrum and *d*-orbitals initially constructed in the dielectric gap. For some parameters of the attracting impurity potentials, the scattering from them leads to a formation of tails in the density of states. It was found that a narrow, continuous band of impurity states could be generated in the gap. This band with a high density of states resulted from hybridization, which led to virtual electronic transitions among impurity states, such as transitions from an initial impurity level to an extended band state, then to another impurity, to a band state, etc. An important point is that the peak of localized states due to a high concentration of impurities is within the band. It was demonstrated that when there is one electron per impurity atom, the nonmagnetic solution described a state with metallic conductivity.

One peculiar feature of oxide dielectrics doped with transitional metals is the strong dependence of the high-energy section of the electron spectrum in the gap on the impurity concentration detected in experiments.^{13–17} A necessary condition of a transition from the insulator to metal is the emergence of a finite density of states in the middle of the dielectric gap.¹⁸ In this case the Fermi level, whose position is weakly affected by the doping, is in the middle of the gap, and the population function of the states formed in the gap apparently has a Fermi character. The data about the quasiparticle spectrum in this band indicate that its states are constructed from those of the host material.

In this paper we will discuss a model which in a sense is intermediate between the lattice and disorder models. The main purpose of our study was to investigate the features of the insulator–metal transition described above in terms of formation of impurity bands from both localized and extended states in strongly correlated systems. We have studied how the band structure of a dielectric doped with magnetic impurities is modified and what is the phase diagram of the system as a function of the impurity concentration. The sys-

tem ground state was derived from Green's functions averaged over configurations of impurities randomly distributed through the dielectric lattice using the Hartree-Fock approximation and self-consistent determination of the Fermi energy. We have found that the self-consistent locations of spin-polarized impurity bands in the dielectric gap and their densities of state and population functions strongly depend on the impurity concentration. Strictly speaking, this dependence controls the collapse of magnetic ordering and phase transitions from magnetic insulator to magnetic metal and then to paramagnetic metal as the impurity concentration increases.

Using this approach, we have studied a simple model of a strongly correlated system which is a proper dielectric doped with a magnetic impurity. Therefore we will not apply our results to specific materials. We will demonstrate, however, that the model yields certain general results that may be employed in interpreting experimental data.

2. MODEL

We use a model in which a nondegenerate level ε_0 of an impurity atom is initially located in the middle of the dielectric gap. For simplicity, we limit our calculations to the single-band approximation for a nonmagnetic dielectric. In our model, this limitation is not essential for the final results, and the technique can be easily generalized to investigate the case of several bands and degenerate impurity levels.¹⁹ Properties of nonmagnetic dielectrics doped with transitional metals are often described in terms of the Anderson Hamiltonian, which we write in the form

$$H = \sum_{\mathbf{k}\sigma} \varepsilon_{\mathbf{k}} a_{\mathbf{k}\sigma}^+ a_{\mathbf{k}\sigma} + \sum_{j\sigma} \varepsilon_0 d_{j\sigma}^+ d_{j\sigma} + \sum_{j\sigma} U n_{j\sigma} n_{j,-\sigma} + \sum_{j,\mathbf{k}\sigma} \{V_{\mathbf{k}j} a_{\mathbf{k}\sigma}^+ d_{j\sigma} + V_{j\mathbf{k}} d_{j\sigma}^+ a_{\mathbf{k}\sigma}\}, \quad (1)$$

where $a_{\mathbf{k}\sigma}$ and $d_{j\sigma}$ are usual annihilation operators, σ is the spin index, \mathbf{k} is the wave vector of an electron in the band state with the energy $\varepsilon_{\mathbf{k}}$, j is the impurity atom number, $V_{\mathbf{k}j}$ is the hybridization matrix element, and U is the constant of interaction between d -electrons in the impurity atom.

The equation with the Hamiltonian in Eq. (1) was solved for in the self-consistent Hartree-Fock approximation using the Green's functions averaged over the ensembles of impurity atoms randomly distributed through the lattice and occupying equivalent sites or interstitial positions in the host lattice. To this end, we introduced a modified resonant level for states with the spin σ , i.e.,

$$\varepsilon_0^\sigma = \varepsilon_0 + U \langle n_{j,-\sigma} \rangle, \quad (2)$$

and a single-particle effective Hamiltonian

$$H_{\text{eff}}^\sigma = \sum_{\mathbf{k}} \varepsilon_{\mathbf{k}} a_{\mathbf{k}\sigma}^+ a_{\mathbf{k}\sigma} + \sum_j \varepsilon_0^\sigma d_{j\sigma}^+ d_{j\sigma} + \sum_{j,\mathbf{k}} \{V_{\mathbf{k}j} a_{\mathbf{k}\sigma}^+ d_{j\sigma} + V_{j\mathbf{k}} d_{j\sigma}^+ a_{\mathbf{k}\sigma}\}, \quad (3)$$

Since the impurity atoms occupy equivalent positions in the lattice, the averaged self-consistent filling factors are independent of j and determined by the following formula:

$$\langle n_{d,\pm\sigma} \rangle = -\frac{1}{\pi} \int_{-\infty}^{E_F} d\omega \operatorname{Im} G_{dd}^{\pm\sigma}(\omega, \langle n_{d,\mp\sigma} \rangle), \quad (4)$$

where E_F is the self-consistent Fermi energy of the system and G_{dd}^σ is the matrix element of the one-particle Green's function diagonal with respect to j in the unperturbed orthonormal basis of wave functions. Since this matrix element is also independent of the impurity number, j , we use the index d in Eq. (4).

The Fermi energy is a function of the number of electrons donated by one impurity. In the case of one electron per impurity, we have the following equation valid at zero temperature:

$$\langle n_{d,-\sigma} \rangle + \langle n_{d,\sigma} \rangle - \frac{1}{\pi N_{im}} \operatorname{Im} \int_{-\infty}^{E_F} d\omega \sum_{\mathbf{k},\sigma} \times (G_{\mathbf{k}\mathbf{k}}^\sigma(\omega, \langle n_{d,-\sigma} \rangle) - G_{\mathbf{k}\mathbf{k}}^{\sigma(0)}(\omega)) = 1. \quad (5)$$

Here N_{im} is the impurity concentration, $G_{\mathbf{k}\mathbf{k}}^\sigma$ is the matrix element of the one-particle Green's function diagonal with respect to \mathbf{k} , and $G^{\sigma(0)}$ is the unperturbed Green's function. Accordingly, $G_{\mathbf{k}\mathbf{k}}^{\sigma(0)}(\varepsilon) = (\varepsilon - \varepsilon_{\mathbf{k}})^{-1}$, $G_{dd}^{\sigma(0)}(\varepsilon) = (\varepsilon - \varepsilon_0^\sigma)^{-1}$, and $\varepsilon = \varepsilon + i0^+$.

If the Green's function is known, Eqs. (4) and (5) completely determine the set of plausible states of the system for an arbitrary impurity concentration. This set of solutions can be classified as magnetic states with $\langle n_{d,\sigma} \rangle \neq \langle n_{d,-\sigma} \rangle$ and nonmagnetic states in which $\langle n_{d,\sigma} \rangle = \langle n_{d,-\sigma} \rangle$ holds. As will be shown below, the latter states correspond to a paramagnetic metal. Since the Hartree-Fock procedure is variational, the real state of the system for a given impurity concentration is found by minimizing the total energy of the system. To this end, we introduce the variation of the total energy per impurity atom:

$$\Delta E = -\frac{1}{\pi N_{im}} \operatorname{Im} \int_{-\infty}^{E_F} \omega d\omega \operatorname{Tr} G(\omega) - U \langle n_{d,-\sigma} \rangle \langle n_{d,\sigma} \rangle - \varepsilon_0 - E_{s,i}, \quad (6)$$

where $E_{s,i}$ is the energy of a band electron in the undoped host material. In treating Eq. (6) one should keep in mind that if the Fermi level coincides with the δ -function of the density of localized states, the contribution of these states to the total energy is determined by the product of the energy of the ordinary pole G_{dd}^σ (see below) by their self-consistent filling factor, which is determined by the solution of the system in Eq. (5) and two equations in (4) for various σ . The one-particle Green's function is derived from Eqs. (2) and (3), as described in the next section.

3. EXPRESSIONS FOR DIAGONAL MATRIX ELEMENTS OF THE SELF-ENERGY PART

In the studied ensemble of impurities, the hybridization matrix element is

$$V_{\mathbf{k}j} = V_{\mathbf{k}d} \Omega^{-1/2} \exp(i\mathbf{k}\mathbf{R}_j), \quad (7)$$

where \mathbf{R}_j is the position of the j th impurity and Ω is the dielectric volume.

The diagonal matrix elements of G can be expressed as

$$G_{\mathbf{k}\mathbf{k}}^{\sigma}(\varepsilon) = (G_{\mathbf{k}\mathbf{k}}^{\sigma(0)-1}(\varepsilon) - \Sigma_{\mathbf{k}\mathbf{k}}^{\sigma}(\varepsilon))^{-1},$$

$$G_{dd}^{\sigma}(\varepsilon) = (G_{dd}^{\sigma(0)-1}(\varepsilon) - \Sigma_{dd}^{\sigma}(\varepsilon))^{-1}, \quad (8)$$

where Σ^{σ} is the self-energy part.

From Eqs. (2) and (3) we derive

$$\Sigma_{\mathbf{k}\mathbf{k}}^{\sigma}(\varepsilon) = \Omega^{-1} G_{dd}^{\sigma(0)} \sum_j |V_{\mathbf{k}d}|^2 + G_{dd}^{\sigma(0)2} \sum_{j,j_1, \mathbf{k}_1 \neq \mathbf{k}} V_{\mathbf{k}j} V_{j \mathbf{k}_1}$$

$$\times G_{\mathbf{k}_1 \mathbf{k}_1}^{\sigma(0)} V_{\mathbf{k}_1 j_1} V_{j_1 \mathbf{k}} + G_{dd}^{\sigma(0)3} \sum_{j_i, \mathbf{k}_i \neq \mathbf{k}} V_{\mathbf{k}j} V_{j \mathbf{k}_1} G_{\mathbf{k}_1 \mathbf{k}_1}^{\sigma(0)} V_{\mathbf{k}_1 j_1}$$

$$\times V_{j_1 \mathbf{k}_2} G_{\mathbf{k}_2 \mathbf{k}_2}^{\sigma(0)} V_{\mathbf{k}_2 j_2} V_{j_2 \mathbf{k}} + \dots \quad (9)$$

Similarly we find

$$\Sigma_{dd}^{\sigma} = \Omega^{-1} \sum_{\mathbf{k}} D_{\mathbf{k}}^{\sigma} |V_{\mathbf{k}d}|^2 + G_{dd}^{\sigma(0)} \sum_{j_1 \neq j, \mathbf{k}_1 \neq \mathbf{k}} D_{\mathbf{k}}^{\sigma} V_{j \mathbf{k}} V_{\mathbf{k} j_1}$$

$$\times D_{\mathbf{k}_1}^{\sigma} V_{j_1 \mathbf{k}_1} V_{\mathbf{k}_1 j} + G_{dd}^{\sigma(0)2} \sum_{j_i \neq j, \mathbf{k}_i \neq \mathbf{k}_{i-1}} D_{\mathbf{k}}^{\sigma} V_{j \mathbf{k}} V_{\mathbf{k} j_1}$$

$$\times D_{\mathbf{k}_1}^{\sigma} V_{j_1 \mathbf{k}_1} V_{\mathbf{k}_1 j_2} D_{\mathbf{k}_2}^{\sigma} V_{j_2 \mathbf{k}_2} V_{\mathbf{k}_2 j} + \dots \quad (10)$$

Here we use the notation

$$D_{\mathbf{k}}^{\sigma}(\varepsilon) = S_{\mathbf{k}}^{\sigma} G_{\mathbf{k}\mathbf{k}}^{\sigma(0)},$$

$$S_{\mathbf{k}}^{\sigma}(\varepsilon) = \left(1 - G_{\mathbf{k}\mathbf{k}}^{\sigma(0)} G_{dd}^{\sigma(0)} \sum_{j_1 \neq j} |V_{\mathbf{k} j_1}|^2 \right)^{-1}. \quad (11)$$

Given Eq. (7), in calculating the sums over j in Eqs. (9) and (10) we should average the result over a random distributions of impurities. To this end, we must calculate the following s th moments:

$$M_s(\mathbf{k}_1, \mathbf{k}_2, \dots, \mathbf{k}_s)$$

$$= \left\langle \sum_{\{n_1\}} \sum_{\{n_2\}} \dots \sum_{\{n_s\}} \exp \left(-i \sum_m \mathbf{k}_m \mathbf{R}_{n_m} \right) \right\rangle_{\text{av}},$$

where $\langle \dots \rangle_{\text{av}}$ denotes averaging over all possible configurations of the impurity ensemble. In order to calculate diagonal matrix elements of the self-energy part averaged over all configurations, we use the Matsubara technique originally designed for alloys.^{20,21}

After straightforward but lengthy calculations, we derive from Eq. (9)

$$\Sigma_{\mathbf{k}\mathbf{k}}^{\sigma}(\varepsilon) = \frac{G_{dd}^{\sigma(0)} N_{im} |V_{\mathbf{k}d}|^2}{1 - G_{dd}^{\sigma(0)} \sum'_{\mathbf{k}_1 \neq \mathbf{k}} |V_{\mathbf{k}_1 d}|^2 G_{\mathbf{k}_1 \mathbf{k}_1}^{\sigma(0)}}$$

$$\times \left(1 - c G_{dd}^{\sigma(0)} \sum'_{\mathbf{k}_2 \neq \mathbf{k}} |V_{\mathbf{k}_2 d}|^2 G_{\mathbf{k}_2 \mathbf{k}_2}^{\sigma(0)} \right.$$

$$+ 2c^2 G_{dd}^{\sigma(0)2} \left(\sum'_{\mathbf{k}_2 \neq \mathbf{k}} |V_{\mathbf{k}_2 d}|^2 G_{\mathbf{k}_2 \mathbf{k}_2}^{\sigma(0)} \right)^2$$

$$\left. - c N_{im} G_{dd}^{\sigma(0)2} \sum'_{\mathbf{k}_2 \neq \mathbf{k}} |V_{\mathbf{k}_2 d}|^4 G_{\mathbf{k}_2 \mathbf{k}_2}^{\sigma(0)2} + \dots \right). \quad (12)$$

Accordingly, Eq. (10) is transformed with due account of Eq. (11) to

$$\Sigma_{dd}^{\sigma}(\varepsilon) = \sum_{\mathbf{k}}' S_{\mathbf{k}}^{\sigma} |V_{\mathbf{k}d}|^2 G_{\mathbf{k}\mathbf{k}}^{\sigma(0)} (1 + N_{im} S_{\mathbf{k}}^{\sigma} |V_{\mathbf{k}d}|^2 G_{\mathbf{k}\mathbf{k}}^{\sigma(0)})$$

$$\times G_{dd}^{\sigma(0)2} ((1-c) F^{\sigma}(\varepsilon) + (1-3c+2c^2) G_{dd}^{\sigma(0)} F^{\sigma^2}$$

$$+ (1-7c+12c^2-6c^3) G_{dd}^{\sigma(0)2} F^{\sigma^3} + \dots), \quad (13)$$

where

$$F^{\sigma}(\varepsilon) = \sum_{\mathbf{k}_1 \neq \mathbf{k}}' S_{\mathbf{k}_1}^{\sigma} |V_{\mathbf{k}_1 d}|^2 G_{\mathbf{k}_1 \mathbf{k}_1}^{\sigma(0)}. \quad (14)$$

In Eqs. (11)–(13) we use the notations

$$\sum_{\mathbf{k}}' \rightarrow \int \frac{d\mathbf{k}}{(2\pi)^3},$$

$$S_{\mathbf{k}}^{\sigma}(\varepsilon, N_{im}) = (1 - G_{\mathbf{k}\mathbf{k}}^{\sigma(0)} G_{dd}^{\sigma(0)} N_{im} |V_{\mathbf{k}d}|^2)^{-1},$$

and $c = N_{im}/N_s$, N_s is the density of sites (interstitial positions) in the dielectric lattice.

In real situations we have $c \ll 1$. From Eqs. (12)–(14) one can derive limitations on the impurity concentration under which only the first terms of the series for $\Sigma_{\mathbf{k}\mathbf{k}}^{\sigma}$ and Σ_{dd}^{σ} need be retained. In this case Eq. (8) determines the diagonal matrix elements of $G^{(1)}$.

The exact Green's function for the effective Hamiltonian (3), certainly satisfies Levinson's theorem, which can be formulated for states with a fixed spin as

$$\text{Im} \int d\varepsilon \text{Tr}(G^{\sigma}(\varepsilon) - G^{\sigma(0)}(\varepsilon)) = 0. \quad (15)$$

Equation (15) signifies that the total number of electronic states for the Hamiltonian (3) is the same as that for the unperturbed Hamiltonian.

In order to check whether the higher-order terms in Eqs. (12) and (13) may be omitted and hence the calculated diagonal matrix elements of the Green's function $G^{\sigma(1)}(\varepsilon)$ are correct, we use the condition

$$\gamma^{\sigma}(N_{im}) = \frac{1}{N_{im}} \text{Im} \int d\varepsilon \text{Tr}(G^{\sigma(1)}(\varepsilon) - G^{\sigma(0)}(\varepsilon)) \ll 1$$

for two fixed spin projections and a fixed impurity concentration.

4. DETAILS OF CALCULATIONS USING THE ONE-BAND DIELECTRIC MODEL

In our calculations, we took the "semielliptic" model of a symmetrical band (for definiteness, the valence band) with a width $2D_b$, the total number of states with a particular spin projection $N_t/2$, and the density of states with a fixed spin

$$\rho_{\text{ext}}^{(0)}(\varepsilon) = \begin{cases} \frac{N_t}{\pi D_b^2} (D_b^2 - \varepsilon^2)^{1/2}, & |\varepsilon| \leq D_b \\ 0, & |\varepsilon| > D_b \end{cases}. \quad (16)$$

Then we assume that $V_{\mathbf{k}d}$ does not change with \mathbf{k} . After substituting the summation over \mathbf{k} with the integration with respect to $\varepsilon_{\mathbf{k}}$ and taking into account Eq. (16), we obtain

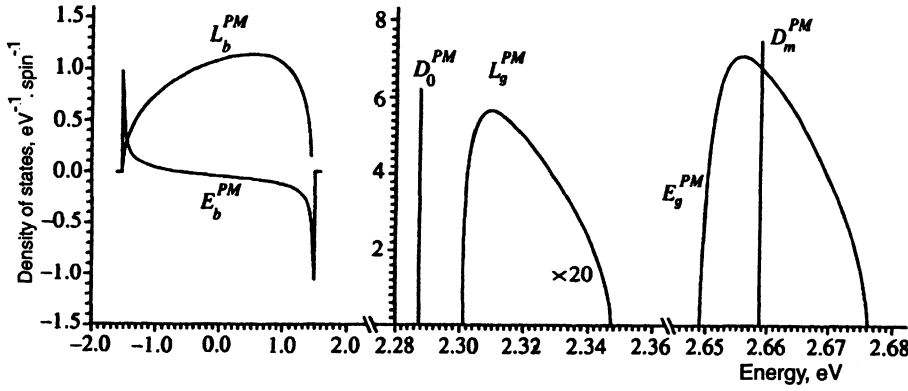


FIG. 1. Diagram of density of states in the paramagnetic metallic state. The curve E_b^{PM} shows the change in the density of states per impurity, $\Delta\rho_{\text{ext}}^{\sigma}(\varepsilon)$. The system parameters are $N_t = 0.07 \text{ \AA}^{-3}$, $D_b = 1.5 \text{ eV}$, $\varepsilon_0 = 2 \text{ eV}$, $x = 0.03$, $V_{kd} \cdot N_t^{1/2} = 1.5 \text{ eV}$, and $U = 0.5 \text{ eV}$.

$$\Sigma_{\mathbf{k}\mathbf{k}}^{\sigma(1)}(\omega) = \frac{N_{im} G_{dd}^{\sigma(0)}(\omega) V_{kd}^2}{1 - \pi G_{dd}^{\sigma(0)} V_{kd}^2 [\beta(\omega) - i\rho_{\text{ext}}^{\sigma(0)}(\omega)]}, \quad (17)$$

$$\Sigma_{dd}^{\sigma(1)}(\omega) = \pi V_{kd}^2 (\beta(\omega^{\sigma}) - i\rho_{\text{ext}}^{\sigma(0)}(\omega^{\sigma})). \quad (18)$$

Here we use the notation $\omega^{\sigma} = \omega - N_{im} G_{dd}^{\sigma(0)} V_{kd}^2$ and

$$\beta(\omega) = \frac{N_t}{\pi D_b^2} \begin{cases} \omega, & |\omega| \leq D_b \\ \omega - \text{sign}(\omega)(\omega^2 - D_b^2)^{1/2}, & |\omega| > D_b. \end{cases} \quad (19)$$

In the general case, the poles of $G_{\mathbf{k}\mathbf{k}}^{\sigma(1)}$ and $G_{dd}^{\sigma(1)}$ may be both in the initial valence band and in the dielectric gap.

Finally, the density of state with a fixed spin defined as

$$\rho_{\text{ext}}^{\sigma}(\omega) = -\frac{1}{\pi} \sum_{\mathbf{k}}' G_{\mathbf{k}\mathbf{k}}^{\sigma(1)}(\omega),$$

is expressed as

$$\rho_{\text{ext}}^{\sigma}(\omega) = \frac{2N_t}{\pi D_b} \text{Im} \left[t \left(1 - \left(\frac{1+t}{t} \right)^{1/2} \right) \right], \quad (20)$$

where

$$t = \frac{-\omega - D_b + \Sigma_{\mathbf{k}\mathbf{k}}^{\sigma(1)}}{2D_b},$$

and the root with $\text{Im}(1 + t/t)^{1/2} \geq 0$ should be chosen.

The density of localized states with a fixed spin, defined as

$$\rho_{\text{loc}}^{\sigma} = -\frac{1}{\pi} N_{im} \text{Im} G_{dd}^{\sigma(1)}(\omega),$$

has the form

$$\rho_{\text{loc}}^{\sigma}(\omega) = N_{im} \begin{cases} -\frac{1}{\pi} \frac{\text{Im} \Sigma_{dd}^{\sigma(1)}(\omega)}{(\omega - \varepsilon_0^{\sigma} - \text{Re} \Sigma_{dd}^{\sigma(1)})^2 + (\text{Im} \Sigma_{dd}^{\sigma(1)})^2}, & |\omega^{\sigma}| \leq D_b \\ \sum_m (A'_{\omega=\omega_m^{\sigma}})^{-1} \delta(\omega - \omega_m^{\sigma}), & |\omega^{\sigma}| > D_b, \end{cases} \quad (21)$$

where the positions of the simple poles, ω_m^{σ} , are the roots of the equation

$$A(\omega) = \omega - \varepsilon_0^{\sigma} - \text{Re} \Sigma_{dd}^{\sigma(1)}(\omega) = 0. \quad (22)$$

In order to clearly demonstrate the effect of impurities on the density of states in the valence band, we introduce the variation in the density of states per impurity atom:

$$\Delta\rho_{\text{ext}}^{\sigma}(\varepsilon) = \frac{\rho_{\text{ext}}^{\sigma} - \rho_{\text{ext}}^{\sigma(0)}}{N_{im}},$$

where $\rho_{\text{ext}}^{\sigma}$ is defined by Eq. (20).

It is convenient to normalize the density of both localized and extended states generated in the dielectric gap to the concentration N_{im} of impurity atoms:

$$\rho_{\text{ext}}^{\sigma}(\varepsilon) = \frac{\rho_{\text{ext}}^{\sigma}}{N_{im}}, \quad \rho_{\text{loc}}^{\sigma}(\varepsilon) = \frac{\rho_{\text{loc}}^{\sigma}}{N_{im}}.$$

In what follows we characterize the impurity ensemble in terms of the relative impurity concentration defined as $x = N_{im}/N_t$. The magnetic ordering parameter is the magnetic moment per impurity atom (in Bohr magnetons μ_B).

5. RESULTS AND DISCUSSION

First of all, we note that in the case of one electron per impurity discussed in this paper, there is a solution which describes a paramagnetic metallic state, in addition to the magnetic insulating state realized at a low impurity concentration. Energy bands of the conducting state at $x = 0.03$ are shown in Fig. 1. In this case we have $\langle n_{d,+ \sigma} \rangle = \langle n_{d,- \sigma} \rangle = 0.575$, so the electron extended states are spin degenerate. The Fermi energy in this state is $E_F = 2.659$. The curve E_b^{PM} in Fig. 1 shows the variation in the density of states with a fixed spin in the valence band per

impurity. Note the tail of the density of states ρ_{ext}^σ below the bottom of the valence band at -1.5 eV. At $x=0.03$ the tail extends ≈ 15 meV from the bottom, but both its range and the number of states in it grow with the impurity concentration. A similar effect takes place in the case of magnetic ordering. We have investigated tails of the density of states due to potential scattering earlier,¹² so we do not discuss these states in this paper.

The function E_b^{PM} versus the energy is highly susceptible to the parameters of the problem. But the general trend with different sets of parameters is that the change in the total number of states with a fixed spin in the valence band (taking the tail into account) per impurity atom, i.e.,

$$\Delta N(E_b^{PM}) = \int d\varepsilon \Delta \rho_{\text{ext}}^\sigma(\varepsilon),$$

is negative. At $x=0.03$ we have $\Delta N(E_b^{PM}) = -0.135$.

The curve L_b^{PM} in Fig. 1 shows the normalized density of localized states in the region of the initial valence band. These states are due to the hybridization between the band states and d -orbitals of the impurity atoms. It is well known that they are generated by the Anderson Hamiltonian even with one impurity atom.¹⁹ The total number of localized states is $N(L_b^{PM}) = 0.134$ per spin per one impurity atom.

The density of electron states deep inside the dielectric gap is also shown in Fig. 1. It contains two δ -functions for localized states. The first one, labeled, by D_0^{PM} , corresponds to the simple pole of $G_{dd}^{(1)}$, whose position coincides with the renormalized resonant level ε_0^σ determined by Eq. (2). At $x=0.03$ the nonmagnetic solution yields $\langle n_{d,\pm\sigma} \rangle = 0.575$ and $\varepsilon_0^\sigma = 2.287$. The amplitude of this pole can be easily derived from Eq. (22):

$$(A'(\varepsilon_0))^{-1} = \frac{1}{1+(2x)^{-1}}. \quad (23)$$

The total number of localized states D_0^{PM} per spin is $N(D_0^{PM}) = 5.660 \cdot 10^{-2}$. Being below the Fermi level, all these states are fully occupied.

In the nonmagnetic case, the position of the second ordinary pole of $G_{dd}^{(1)}$ labeled by D_m^{PM} in Fig. 1 coincides with the self-consistent Fermi level of the system, E_F . This pole is located near the middle of the narrow band of continuous states of a high density, E_g^{PM} , due to the poles of $G_{kk}^{(1)}(\varepsilon)$. This location of the pole D_m^{PM} inside the band E_g^{PM} is a common feature of band patterns at $V_{kd}=0$, irrespective of other parameters. The total number of localized states D_m^{PM} per spin per impurity atom is $N(D_m^{PM}) = 0.80$, and their self-consistent filling factor per spin is 0.375.

The band E_g^{PM} is generated only when the hybridization matrix elements V_{kd} are nonzero. This band of extended states is caused by the motion of charge carriers across a random ensemble of impurities (hence across the crystal) due to the virtual electronic transitions from the initial impurity atom to a band state, then to another impurity, to another band state and so on. In the pattern of energy bands given in Fig. 1 the width of the band E_g^{PM} is $\Delta_g \approx 27$ meV, and the

total number of states per spin per impurity is $N(E_g^{PM}) = 0.135$. From these figures we derive the average density of states in this band:

$$\langle \rho_{\text{ext}}(E_g^{PM}) \rangle = 2N_{im} \frac{N(E_g^{PM})}{\Delta_g} \approx 0.21 \cdot 10^{23} \text{ cm}^{-3} \cdot \text{eV}^{-1}.$$

The Fermi level is located inside the band E_g^{PM} and determines the filling factor of this band of extended states equal to 0.44. The transport characteristics of this conducting state are unusual since the density of unoccupied localized states on the Fermi level is high (as was noted above, the filling factor of D_m^{PM} states is 0.375). But in this paper we will not dwell on this topic.

The band pattern modified by doping also includes a band of localized states L_g^{PM} around the renormalized resonant d -level shown in Fig. 1. In the case under discussion, the total number of these localized states per spin per impurity is $N(L_g^{PM}) = 0.933 \cdot 10^{-2}$ and, being below the Fermi level, all these states are occupied.

Note that in the modified band structure shown in Fig. 1 Levinson's theorem is satisfied with an accuracy $\gamma^\sigma = 0.9 \cdot 10^{-6}$.

In the paramagnetic metallic state the variation in the total energy per impurity is $\Delta E^{PM} = -0.250$ eV at $x=0.03$. This parameter is higher than in the case of the magnetic insulator, $\Delta E^{MI} = -0.321$ eV. Since we have used the variational procedure, at the impurity concentration corresponding to $x=0.03$ the magnetic insulating state is realized. Then the self-consistent filling factors are $\langle n_{d,+ \sigma} \rangle = 1$ and $\langle n_{d,- \sigma} \rangle = 0.116$ (the case of the symmetrical solution with $\sigma \rightarrow -\sigma$ is not of interest). As a result of the inequality between the filling factors, the initially spin degenerate valence band is modified by being split into two spin-polarized bands of extended states whose spectrum is determined by poles of $G_{kk}^{\sigma(1)}$. The energies of these two subbands are almost equal. Two spin-polarized bands of localized states are also generated in the valence band. The density of states in these bands is similar to that shown in Fig. 1, so they are not plotted in Fig. 2. We quote only the variations in the total numbers of states in these bands at $x=0.03$: $\Delta N(E_{b,+ \sigma}^{MI}) = -0.160$, $\Delta N(E_{b,- \sigma}^{MI}) = -0.116$, $N(L_{b,+ \sigma}^{MI}) = 0.159$, $N(L_{b,- \sigma}^{MI}) = 0.116$. Hence it follows that the total magnetic moment in these bands per impurity is $0.8 \cdot 10^{-3}$ Bohr magneton.

The impurity bands in the magnetic insulating state in the dielectric gap at $x=0.03$ are shown in Fig. 2. Their origin is similar to that of the bands in Fig. 1. But unlike the case of paramagnetic metal, they are spin-split, and the subbands with different spin projections are labelled by the index σ in the diagram. The Fermi energy in this case is $E_F = 2.5$ eV, which corresponds to the δ -peak of localized states $D_{0,- \sigma}^{MI}$. The total numbers of states in the bands, $D_{0,- \sigma}^{MI}$ and $D_{0,+ \sigma}^{MI}$ (the latter is fully occupied), depends only on the impurity concentration x and is determined by Eq. (23). The filling factor in the $D_{0,- \sigma}^{MI}$ band is much less than unity and equals $0.344 \cdot 10^{-2}$. The following occupied bands are located be-

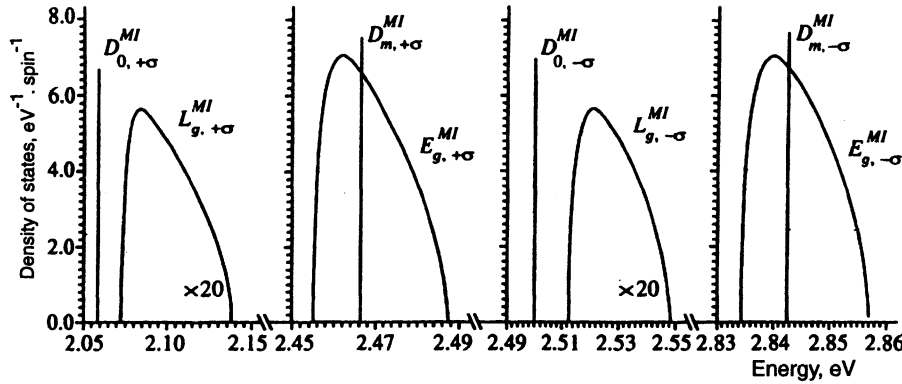


FIG. 2. Diagram of bands in the dielectric gap in the magnetic insulating state. The lower index $I \pm \sigma$ indicates spin splitting of impurity bands. The system parameters are the same as in Fig. 1.

low the Fermi level: the band of localized states $L_{g,+σ}^{MI}$ with a total number of states per impurity of $0.128 \cdot 10^{-1}$; the band of extended states $E_{g,+σ}^{MI}$ with a total number of states per impurity of 0.160, and a δ -peak of localized states $D_{m,+σ}^{MI}$ with a total number of states per impurity of 0.772 in the middle of the previous band.

Figure 2 shows that a gap of 13 meV separates the localized states $D_{0,-σ}^{MI}$ on the Fermi level from the empty band of localized electron states $L_{g,-σ}^{MI}$ with a total number of states per impurity atom of $0.730 \cdot 10^{-2}$. Across a gap of 0.334 eV above this band, there is a spin-polarized band of extended states $E_{g,-σ}^{MI}$ with a total number of states per impurity of 0.116 and a δ -peak of localized states $D_{m,-σ}^{MI}$, which has 0.820 states per impurity, in the middle of the extended band. At $x=0.03$, the total magnetic moment per impurity in the magnetic insulating state is $M=1\mu_B$. The calculation accuracy for the states with spin $+\sigma$ is worse: $\gamma^{+\sigma}=0.7 \cdot 10^{-5}$.

The self-consistent positions of the impurity bands generated in the dielectric gap, and their densities of states and filling factors strongly depend on the impurity concentration. In the long run this dependence controls the phase transitions taking place in the system as the impurity concentration is increased. The transformation of impurity bands due to the magnetic insulator–magnetic metal transition is shown in Fig. 3. It shows only the high-energy section of the spectrum with four impurity bands around the Fermi level at three impurity concentrations (the intermediate insulating state is illustrated by Fig. 2). In the insulating state the gap between the top of the full band of extended states $E_{g,+σ}^{MI}$ and the

partially filled band of localized states $D_{0,-σ}^{MI}$ drops with x , as seen in Figs. 2 and 3a. The positions of E_F and $D_{0,-σ}^{MI}$ are constant till the localized states with the spin $+\sigma$ are full and $\langle n_{d,+σ} \rangle = 1$. When the band $E_{g,+σ}^{MI}$ shifts towards E_F , it overlaps with the partially filled $D_{0,-σ}^{MI}$ band at $x \approx 0.04$, as shown in Fig. 3b. At $x=0.044$ (Fig. 3c) the Fermi level is in the band of extended states $E_{g,+σ}^{MM}$ and near the peak of $D_{m,+σ}^{MM}$, so the system transforms to a magnetic metal with a magnetic moment per impurity of $0.839\mu_B$. We assume that the impurity concentration corresponding to the insulator–metal transition is determined by the overlap between the extended and localized bands. The pattern of other impurity bands in the metallic state, except those shown in Fig. 3c, is similar to that of the insulating state given in Fig. 2.

At each impurity concentration given in Fig. 3 there is also a solution describing a paramagnetic conducting state. Its band pattern is similar to that shown in Fig. 1, but this state is not realized at these concentrations because of the minimum energy condition. In what follows, only the energy of this state will be given in this concentration range.

At higher x there are two solutions for the system, namely the magnetic and paramagnetic metallic states. The transformation of impurity bands around the Fermi level due to the transition from the magnetic to paramagnetic metal is shown in Fig. 4. As x increases, the Fermi level, which controls the density of free carriers with the spin $+\sigma$ in the band $E_{g,+σ}^{MM}$, becomes closer to the level $D_{m,+σ}^{MM}$ in the middle of this band. As long as the states $E_{g,-σ}^{MM}$ are occupied, carriers with spin $-\sigma$ are localized, and the charge transport in the

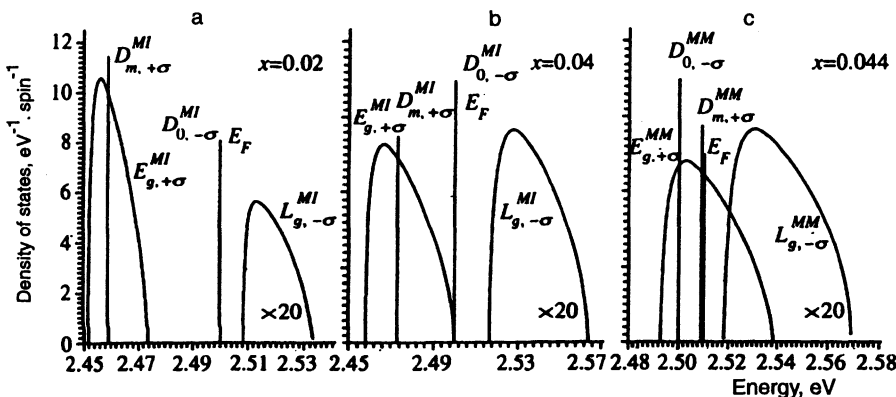


FIG. 3. Transformation of impurity bands as a function of impurity concentration around the Fermi level in the magnetic insulator–magnetic metal transition. The system parameters, except x , are the same as in Fig. 1: a) insulating state; b) point of transition from magnetic insulator to magnetic metal; c) conducting state.

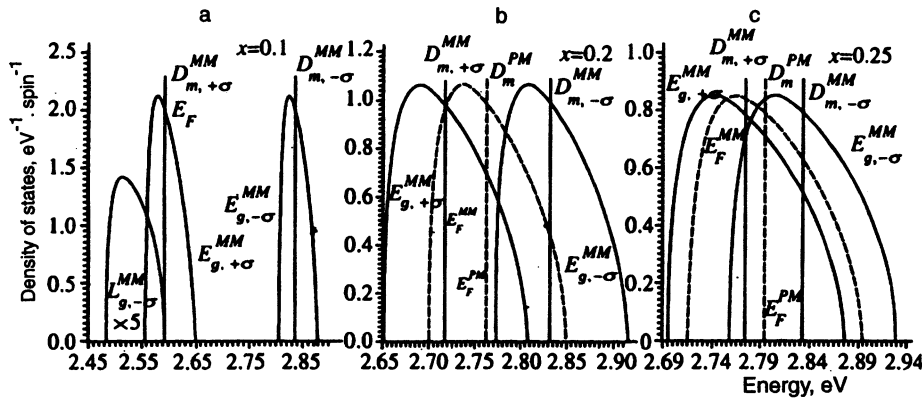


FIG. 4. Transformation of impurity bands around the point of transition from the magnetic metallic to paramagnetic metallic state. Only the bands near the Fermi level are shown. The system parameters, except x , are the same as in Fig. 1: a) $x=0.10$; b) $x=0.20$; c) $x=0.25$.

band of extended states $E_{g,+σ}^{MM}$ leads to the transport of spin $+σ$. You can see in Fig. 4a that the Fermi energy at $x=0.1$ is determined by the states $D_{m,+σ}^{MM}$, whose self-consistent filling factor is smaller than unity, namely 0.822. The localized states $D_{0,-σ}^{MM}$ and $L_{g,-σ}^{MM}$ are totally occupied. The magnetic moment per impurity atom decrease as a function of x to $0.619μ_B$ at $x=0.1$. In this case $γ^{+σ}=1.2 \cdot 10^{-4}$ is the maximum value.

At higher x the spin subbands of extended states, $E_{g,+σ}^{MM}$ and $E_{g,-σ}^{MM}$, become closer. At $x=0.1$ the gap between them is 156 meV (Fig. 4a), whereas at $x=0.05$ it equals 277 meV. The overlap of these spin subbands at $x=0.2$ is shown in Fig. 4b. The dashed line in this diagram shows the bands E_g^{PM} and D_m^{PM} of the paramagnetic metal at the same concentration. The nonmagnetic state is not realized because its energy $ΔE^{PM} = -0.363$ eV is higher than that of the magnetic state, $ΔE^{MM} = -0.371$ eV. The band $E_{g,-σ}^{MM}$ is not occupied since it is higher than the Fermi level pinned to the level $D_{m,+σ}^{MM}$, whose filling factor is 0.488. At $x=0.2$ the magnetic moment per impurity atom is $0.331μ_B$ and the accuracy is $γ = -1.3 \cdot 10^{-3}$.

The situation when the band $E_{g,-σ}^{MM}$ is partially filled at $x=0.25$ is shown in Fig. 4c. The self-consistent filling factors of the states in the magnetic metal are close: $\langle n_{d,+σ} \rangle = 0.651$ and $\langle n_{d,-σ} \rangle = 0.503$. The filling factor of the $D_{m,+σ}^{MM}$ band monotonically drops with x and equals 0.285 at $x=0.25$. In this case the magnetic moment per impurity atom is $0.203μ_B$ with spin-polarized bands around the va-

lence band and in the original dielectric gap taken into account. In the paramagnetic metal we have $\langle n_{d,+σ} \rangle = \langle n_{d,-σ} \rangle = 0.553$ and the filling factor of states in D_m^{PM} band per spin per impurity atom is considerably smaller, namely $4.41 \cdot 10^{-2}$. The overlap between spin subbands of extended states, $E_{g,+σ}^{MM}$ and $E_{g,-σ}^{MM}$, increases with x ; as a result, first the filling factor of the subband $E_{g,-σ}^{MM}$ grows, since it includes the Fermi level controlled by the level $D_{m,+σ}^{MM}$, and then the states $D_{m,-σ}^{MM}$ are occupied at the expense of $D_{m,+σ}^{MM}$. Consequently the magnetic ordering in the system vanishes and the modified density of states becomes spin-degenerate.

At $x=0.25$ the variation in the total energy per impurity in the magnetized state, $ΔE^{MM} = -0.387$ eV, is slightly lower than in the paramagnetic state, $ΔE^{PM} = -0.385$ eV, whose density of states around the Fermi level is shown in Fig. 4b by the dashed line. The accuracy is $γ = -0.85 \cdot 10^{-3}$. At $x=0.27$ the energies of the magnetic and nonmagnetic states are equal, $ΔE^{PM} = -0.393$ (in this calculation we have $γ = -1.2 \cdot 10^{-2}$). The bands $E_{g,+σ}^{MM}$, $E_{g,-σ}^{MM}$, and E_g^{PM} almost coincide. Therefore we estimate the impurity concentration of the transitions from the magnetic to paramagnetic metal at $x=0.27$. At larger x there is only one solution describing the paramagnetic state whose pattern of energy bands is similar to that shown in Fig. 1.

The resulting phase diagram, energies of states calculated by solving Eqs. (2)–(6) versus impurity concentration, and the magnetic-order parameter versus impurity concentra-

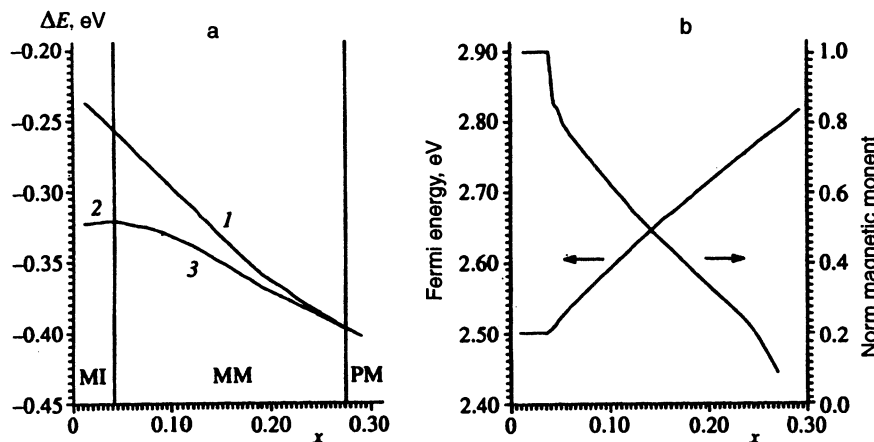


FIG. 5. (a) Phase diagram of the system and energies of paramagnetic metallic (curve 1), magnetic insulating (curve 2) and magnetic metallic (curve 3) states versus relative impurity concentration. (b) Magnetic-order parameter and self-consistent Fermi energy versus impurity concentration.

tion are plotted in Fig. 5. The curve 2, 3 in Fig. 5a shows the energy of the ground state versus impurity concentration. Its low-concentration portion 2 corresponds to the magnetic insulating state, in which ΔE^{MI} rises with x , whereas E_F and magnetic moment are constant (Fig. 5b). At an impurity concentrations higher than 0.04, i.e., after the magnetic insulator–magnetic metal transition, both ΔE^{MM} (curve 3 in Fig. 5a) and magnetic moment of the metallic state (Fig. 5b) decrease with x . The abrupt change in the magnetic moment above $x=0.04$ is due to the filling of the density-of-states δ -peak in $D_{0,-\sigma}^{MM}$ (Fig. 3b and c). At higher impurity concentrations the magnetic moment drops to zero and the curve of the energy of the paramagnetic state (curve 1 in Fig. 5a) converges with that for the magnetized state, ΔE^{MM} (curve 3 in Fig. 5a), so the phase transition between them is continuous. At $x \geq 0.27$ there is only one solution describing a paramagnetic metallic state. Note that throughout the concentration range the Fermi energy varies within 10%, as can be seen in Fig. 5b.

6. CONCLUSION

We summarize as follows. First, unusual transport properties of the system in the conducting state may be expected. In ordinary metals, scattering of electrons, for example, by phonons leads to transitions to states of the continuous spectrum near the Fermi level. In our case there is a high density of vacant localized states near the Fermi level (the peak of D_m^{PM}). Therefore the scattering of electrons should transfer them not only to extended (E_g^{PM}), but also to localized states so that they no longer contribute to the conductivity. This should affect, for example, the temperature dependence of the conductivity.

Second, optical transitions between the valence band and impurity or between impurity bands in the insulating state should generate optical bands of peculiar shapes due to the narrow empty band of localized states $D_{0,-\sigma}^{MI}$ (in reality it has a finite width) in the middle of the wider empty band of extended states $E_{g,-\sigma}^{MI}$. Given the simple relation between the dipole correlator and optical band shape, we should expect that the narrow band due to the localized states will be determined by a slow dipole decay, and the spectrum due to

$E_{g,-\sigma}^{MI}$ by a fast dipole decay. As a result, a coherent optical response (like the photon echo) may be detected in dielectrics doped with rare-earth metals. Under an external electric field, the coherent optical response should lead to a photo-conductivity due to the band of extended states, which is a nonexponential function of temperature.

Third, the density of extended states in $E_{g,\sigma}$ bands is very high. The estimates were given above. In the conducting state the Fermi level is in this band. The search for a superconducting transition related to impurity bands in such materials is a matter for further study.

We express our gratitude to the International Science Foundation (Grant MFD300) for partial financial support of this work.

- ¹N. F. Mott, *Metal–Insulator Transitions*, Taylor and Francis, London (1990).
- ²D. Belitz and T. R. Kirkpatrick, *Rev. Mod. Phys.* **66**, 261 (1994).
- ³É. Z. Kuchinskii, M. V. Sadovskii, V. G. Suvorov, and M. A. Arkabaev, *Zh. Éksp. Teor. Fiz.* **107**, 2027 (1995) [*JETP* **80**, 1122 (1995)].
- ⁴B. Ammon, M. Troyer, and H. Tsunetsugu, *Phys. Rev. B* **52**, 629 (1995).
- ⁵R. Preuss, W. Hanke, and W. Linden, *Phys. Rev. Lett.* **75**, 1344 (1995).
- ⁶Yu. A. Izyumov, B. M. Letfulov, and E. V. Shipitsyn, *Zh. Éksp. Teor. Fiz.* **105**, 1357 (1994) [*JETP* **79**, 731 (1994)].
- ⁷A. N. Andriotis, E. N. Economou, Q. Li, and C. V. Soukoulis, *Phys. Rev. B* **47**, 9208 (1993).
- ⁸M. A. Tusch and D. E. Logan, *Phys. Rev. B* **48**, 14843 (1993).
- ⁹D. Domingues and C. Wiecko, *Phys. Rev. B* **47**, 10888 (1993).
- ¹⁰C. Dasgupta and J. W. Halley, *Phys. Rev. B* **47**, 1126 (1993).
- ¹¹M. Milovanovic, S. Sachdev, and R. N. Bhatt, *Phys. Rev. Lett.* **63**, 82 (1989).
- ¹²A. I. Agafonov and E. A. Manykin, *Phys. Rev. B* **52**, 14571 (1995).
- ¹³H. Eskes, M. B. J. Meinders, and G. A. Sawatzky, *Phys. Rev. Lett.* **67**, 1035 (1991).
- ¹⁴K. Kumagai, T. Suzuki, Y. Taguchi *et al.*, *Phys. Rev. B* **48**, 7636 (1993).
- ¹⁵H. Ohta, T. Takahashi *et al.*, *Phys. Rev. B* **39**, 7354 (1989).
- ¹⁶S. W. Robey, L. T. Hudson, C. Eylem, and B. Eichorn, *Phys. Rev. B* **48**, 562 (1995).
- ¹⁷H. Takagi, T. Ido, S. Ishibashi, M. Uota, and S. Uchida, *Phys. Rev. B* **40**, 2254 (1989).
- ¹⁸G. M. Eliashberg, in *Physical Properties of High Temperature Superconductors*, ed. by D. M. Ginsberg, World Scientific, Singapore (1989).
- ¹⁹F. D. M. Haldane and P. W. Anderson, *Phys. Rev.* **13**, 2553 (1976).
- ²⁰F. Yonezawa and T. Matsubara, *Prog. Theor. Phys.* **35**, 357 (1966).
- ²¹J. Moneske, J. Kortus, and W. Cordts, *Phys. Rev. B* **47**, 9377 (1993).

Translation provided by the Russian Editorial office.